buildings

MDPI

Article

Some Issues in the Seismic Assessment of Shear-Wall Buildings through Code-Compliant Dynamic Analyses

Maria Cristina Porcu [1,*], Juan Carlos Vielma Pérez [2], Gavino Pais [3], Diego Osorio Bravo [3] and Juan Carlos Vielma Quintero [2]

[1] Department of Civil Engineering, Environmental Engineering and Architecture, University of Cagliari, 09123 Cagliari, Italy
[2] Civil Engineering School, Pontificia Universidad Católica de Valparaíso, Valparaíso 2340000, Chile; juan.vielma@pucv.cl (J.C.V.P.); juan.vielma.q@mail.pucv.cl (J.C.V.Q.)
[3] Independent Researcher, Valparaíso 2340000, Chile; paisgavino21@gmail.com (G.P.); diego.osorio.b@mail.pucv.cl (D.O.B.)
* Correspondence: mcporcu@unica.it

Abstract: Due to their excellent seismic behavior, shear wall-type concrete buildings are very popular in earthquake-prone countries like Chile. According to current seismic regulations, the performance of such structures can be indifferently assessed through linear or non-linear methods of analysis. Although all the code-compliant approaches supposedly lead to a safe design, linear approaches may be in fact less precise for catching the actual seismic performance of ductile and dissipative structures, which can even result in unconservative design where comparatively stiff buildings like reinforced-concrete shear-wall (RC-SW) buildings are concerned. By referring to a mid-rise multistory RC-SW building built in Chile and designed according to the current seismic Chilean code, the paper investigates the effectiveness of the linear dynamic analyses to predict the seismic performance of such kind of structures. The findings show that the code-compliant linear approaches (Modal Response Spectrum Analysis and Linear Time-History Analysis) may significantly underestimate the displacement demand in RC-SW buildings. This is highlighted by the comparison with the results obtained from the Non-Linear Time-History Analysis, which is expected to give more realistic results. A set of ten spectrum-consistent Chilean earthquakes was considered to carry out the time-history analyses while a distributed-plasticity fiber-based approach was adopted to model the non-linear behavior of the considered building. The paper highlights how the risk of an unsafe design may become higher when reference is made to the Chilean code, the latter considering only the Modal Response Spectrum Analysis (MRSA) without even providing corrective factors to estimate the inelastic displacement demand. The paper checks the effectiveness of some amplifying factors taken from the literature with reference to the case-study shear-wall building, concluding that they are not effective enough. The paper also warns against the danger of local soft-story collapse mechanisms, which are typical of reinforced concrete frames but may also affect RC-SW buildings when weaker structural parts made by column-like walls are present at the ground floor.

Keywords: effectiveness of seismic linear analysis; non-linear dynamic analysis; reinforced-concrete shear walls; performance-based design

Citation: Porcu, M.C.; Vielma Pérez, J.C.; Pais, G.; Osorio Bravo, D.; Vielma Quintero, J.C. Some Issues in the Seismic Assessment of Shear-Wall Buildings through Code-Compliant Dynamic Analyses. *Buildings* **2022**, *12*, 694. https://doi.org/10.3390/buildings12050694

Academic Editors: Radu Vacareanu and Florin Pavel

Received: 14 April 2022
Accepted: 17 May 2022
Published: 23 May 2022

1. Introduction

Beam-column frames are the most popular type of earthquake-resistant reinforced-concrete buildings. As an exception to this general trend, almost all Chilean residential multistory buildings are made of reinforced-concrete shear walls. Reinforced-concrete shear-wall (RC-SW) buildings, in fact, have been showed to have an excellent performance under violent ground motions, experiencing generally limited damage [1–3]. A well-conducted seismic design is, of course, essential to ensure such a good performance.

Linear and non-linear methods of analysis are currently allowed by codes [4–7] to design earthquake-resistant buildings. As another exception, Chilean regulations [8] only refer to the Modal Response Spectrum Analysis (MRSA). Based on the dynamic equilibrium of forces and on a linear-elastic behavior of the system, the MRSA is often assumed as a reference method for the seismic design of buildings in earthquake-prone regions throughout the world. By combining the maximum contribution of the more significant modes, taken from the design response spectrum, this method introduces some approximations in the evaluation of the seismic demand. A more precise linear approach is the Linear Time-History Analysis (LTHA), which is based on the numerical integration of the motion equations of a linear-elastic system under spectrum-consistent earthquakes. Linear analyses, however, were found to have some limitations in capturing the actual behavior of RC-SW buildings [2], since structures are typically designed to withstand in the elastic range only a reduced level of seismic forces, while relying on their inelastic deformation capacity to withstand higher levels of demand under very strong ground motions.

In fact, structural systems typically exhibit a non-linear behavior under exceptional actions like strong earthquakes [9–11]. This inelastic behavior entails beneficial effects due to the large amount of energy that can be dissipated during the hysteresis loops, so much so that a ductile and dissipative structural behavior is the basis of the modern design philosophy. Accordingly, non-linear methods of analysis have been introduced by most of the current seismic regulations. Among them, the Non-Linear Time-History Analysis (NLTHA) can be considered as the most comprehensive method to assess the behavior of existing, retrofitted, or new buildings under spectrum-consistent earthquakes [12–16]. Non-linear dynamic analyses are in fact shown to better predict the behavior of RC-SW buildings under strong cyclic loads [17–19].

Despite the evidence that almost all civil structures exhibit a non-linear behavior under strong earthquakes, the current regulations generally allow the designer to perform either linear or non-linear seismic analyses, with all the code-compliant approaches supposedly leading to a safe design. Yet, when comparatively stiff structures like RC-SW buildings are concerned, linear approaches may lead to an underestimation of the actual inelastic displacement demand. By exploiting the code-compliant dynamic methods of analysis, the present paper will investigate this matter.

It is of note that linear analyses may be able to estimate the inelastic peak displacements of flexible enough structures behaving like inelastic oscillators under a given strong ground motion rather well. This agrees with the well-known equal-displacement (ED) empirical rule, proved to be valid for low-frequency (typically less than 2 Hz) single-degree-of-freedom (SDOF) systems [20]. The ED rule was found to no longer be met when stiffer SDOF are involved instead. An equal-energy (EE) rule, based on equating elastic and inelastic areas in the force-displacement diagrams, was in fact empirically found to be better able to predict the inelastic peak displacement of stiffer inelastic oscillators [20]. Figure 1 recalls schematically the well-known ED and EE rules for SDOF elastic and elastic-plastic oscillators.

Due to their remarkable stiffness, RC-SW buildings have generally a comparatively high fundamental frequency, which means that the elastic peak displacements are expected to underestimate the actual inelastic displacement demand, according to what discussed above. It is of note that this is not in contrast with the experimental findings presented in [21] where multi-story reinforced concrete walls were found to meet the equal-displacement rule. In fact, the reduced-scale walls tested in [21] were structural systems much less stiff than the whole RC-SW building system to which they actually belonged.

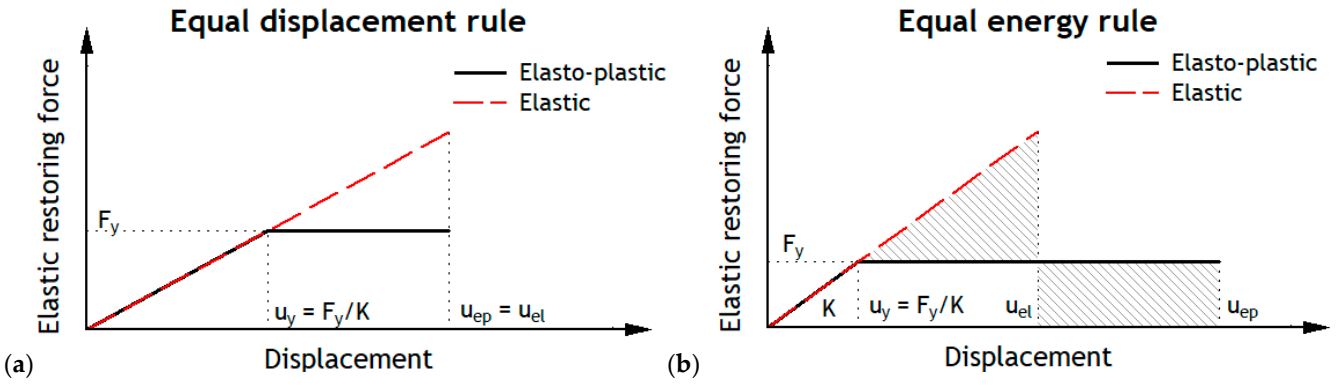

Figure 1. Well-known (**a**) equal displacement and (**b**) equal energy empirical rules relating the peak displacements of elastic and inelastic SDOF oscillators.

It should also be noted that the empirical ED and EE rules were widely investigated for SDOF systems, while their ability to predict the inelastic displacement demand in multi-degree-of-freedom systems has not yet been definitively assessed, although the results of many studies contribute to their extension and generalization. For instance, a numerical study presented in [22] showed that very similar values of maximum elastic and inelastic displacements are attained when historical masonry towers (which are typically characterized by a comparatively long fundamental period) are investigated through time-history linear and non-linear analyses under given earthquakes.

In other words, where sufficiently flexible structures are concerned, performing a linear or a non-linear analysis can be almost indifferent, at least in terms of seismic displacement demand assessment. On the contrary, when much stiffer structures like RC-SW buildings are concerned, the choice between a linear or a non-linear analysis may be anything but indifferent. To avoid an unsafe design, in fact, some codes [4,5] provide the designer empirical factors to evaluate the inelastic displacement demand from the elastic displacements predicted through the MRSA. Such factors are derived from the ED or the EE rules. It is worth noting that the current release of the Chilean code [8] on one hand refers only to the MRSA, and on the other hand does not provide corrective factors to evaluate the inelastic displacement demand from the linear estimated one.

By referring to a case-study (an RC-SW building recently built in Chile), the present paper compares the results obtained from dynamic linear (MRSA and LTHA) and non-linear analyses (NLTHA). A set of ten spectrum-consistent Chilean earthquakes is considered for this purpose, while the building was discretized through a distributed-plasticity fiber-based approach. The averaged values of the maximum displacements and interstory drifts taken from the time-history analyses are compared to those obtained from the MRSA. The effectiveness of some conventional corrective factors proposed in the literature to estimate the peak displacements from the MRSA is checked. A comparison between the results of LTHA and NLTHA is also provided. The paper finally investigates the post-elastic behavior and collapse mechanisms of the considered RC-SW building.

The findings of the present study are expected to have a meaningful impact on the design of RC-SW buildings, this being of paramount importance in countries like Chile where almost 77% of the buildings built from 1940 onwards are RC-SW buildings, most of which are residential constructions ranging from 5 to 25 stories [23]. The aim of the paper is to provide insights about the different seismic assessments that can be achieved though linear and non-linear dynamic analyses when comparatively stiffer structures like RC-SW buildings are concerned. The results of the paper are expected to contribute to the improvement of the current code provisions to achieve a safer design of RC-SW buildings.

2. Case-Study RC-SW Building

A residential complex recently built in the city of Quillota (Chile) was taken as a case-study (see Figure 2a,b). It is a multi-story reinforced concrete building made by shear walls

and designed through linear analyses, accordingly to the Chilean code NCh433 [8]. Located about 50 km from Valparaiso and 130 km from Santiago, Quillota falls into the highest seismicity band of the three in which Chile has been divided by seismic regulations (see Figure 2c), which means that it falls into one of the most seismic-prone areas of the world.

Figure 2. (**a**,**b**) Case-study building in the city of Quillota (**c**) seismic zones in central Chile. In the seismic map, Chile is divided into three bands numbered from 1 to 3, the latter being the higher seismic hazard band, to which Quillota belongs and (**d**) Details of the shear walls reinforcement.

The building is a typical earthquake-resistant Chilean residential RC-SW multistory structure. It is made of reinforced concrete load-bearing shear walls with thickness of 0.20 m, slabs with thickness of 0.16 m, and upturned beams with inverted T or L sections, the web of which is 0.20 m wide. In addition to shear walls, a further typical structural feature of Chilean buildings are the upturned beams, the main function of which is a stiffer connection between walls. In the considered building, upturned beams run along all the perimeter of the structure.

A 3D rendering of the building together with elevation and plan views are displayed in Figure 3, where shear walls are colored in green and upturned beams in red. The plan in Figure 3c evidences the typical "fish bone" Chilean scheme [23], with a longitudinal central corridor and shear walls in the longitudinal and transversal directions that separate the apartments. The walls' pattern recalls a fish bone. Some constructive details of shear wall and upturned beams are displayed in Figure 4. The properties of concrete and reinforcement steel are listed in Tables 1 and 2.

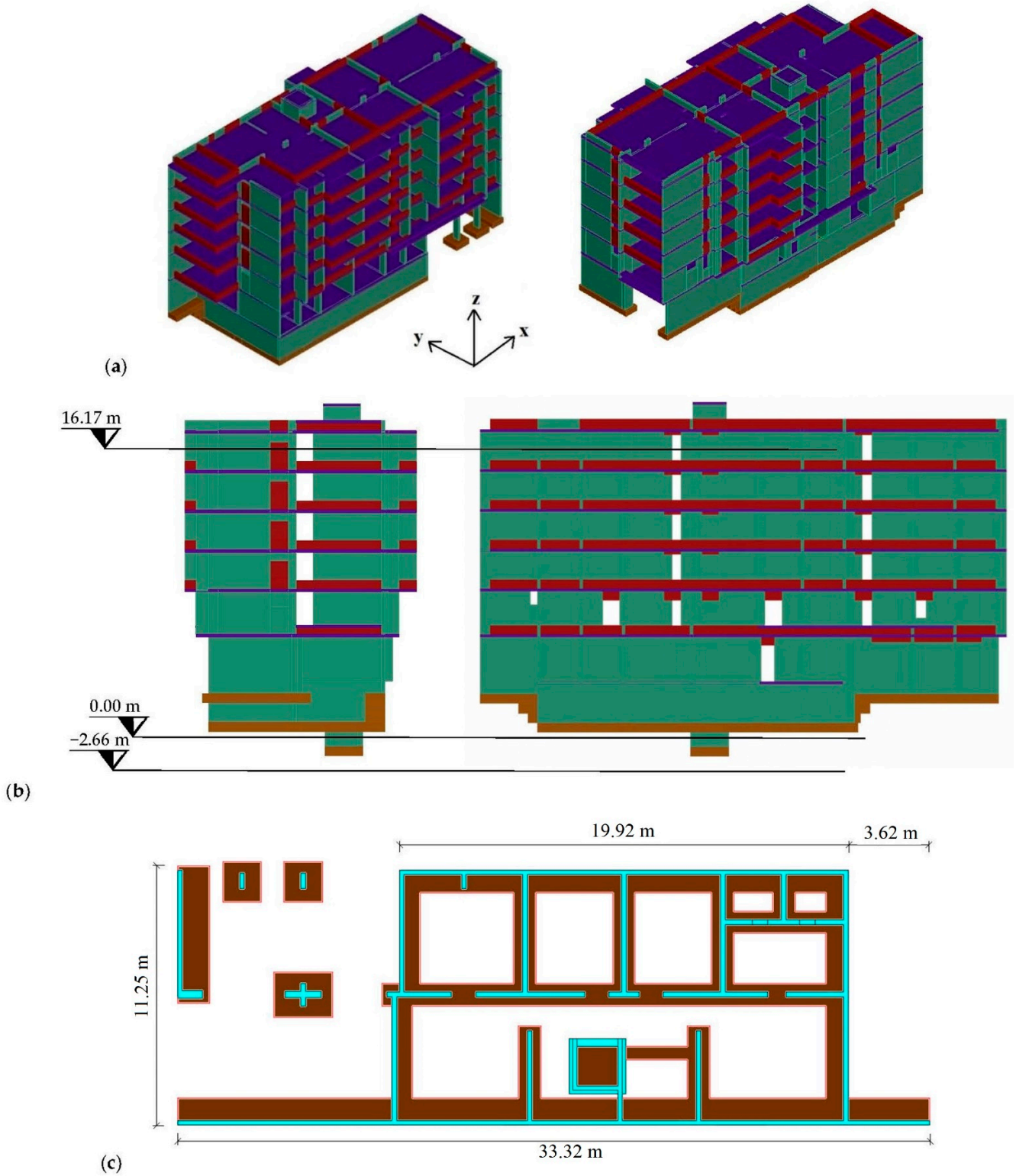

Figure 3. Overall views with the different structural components: (**a**) 3D rendering views; (**b**) elevation sections, and (**c**) plan of the building. Shear walls and upturned beams are colored in green and red, respectively.

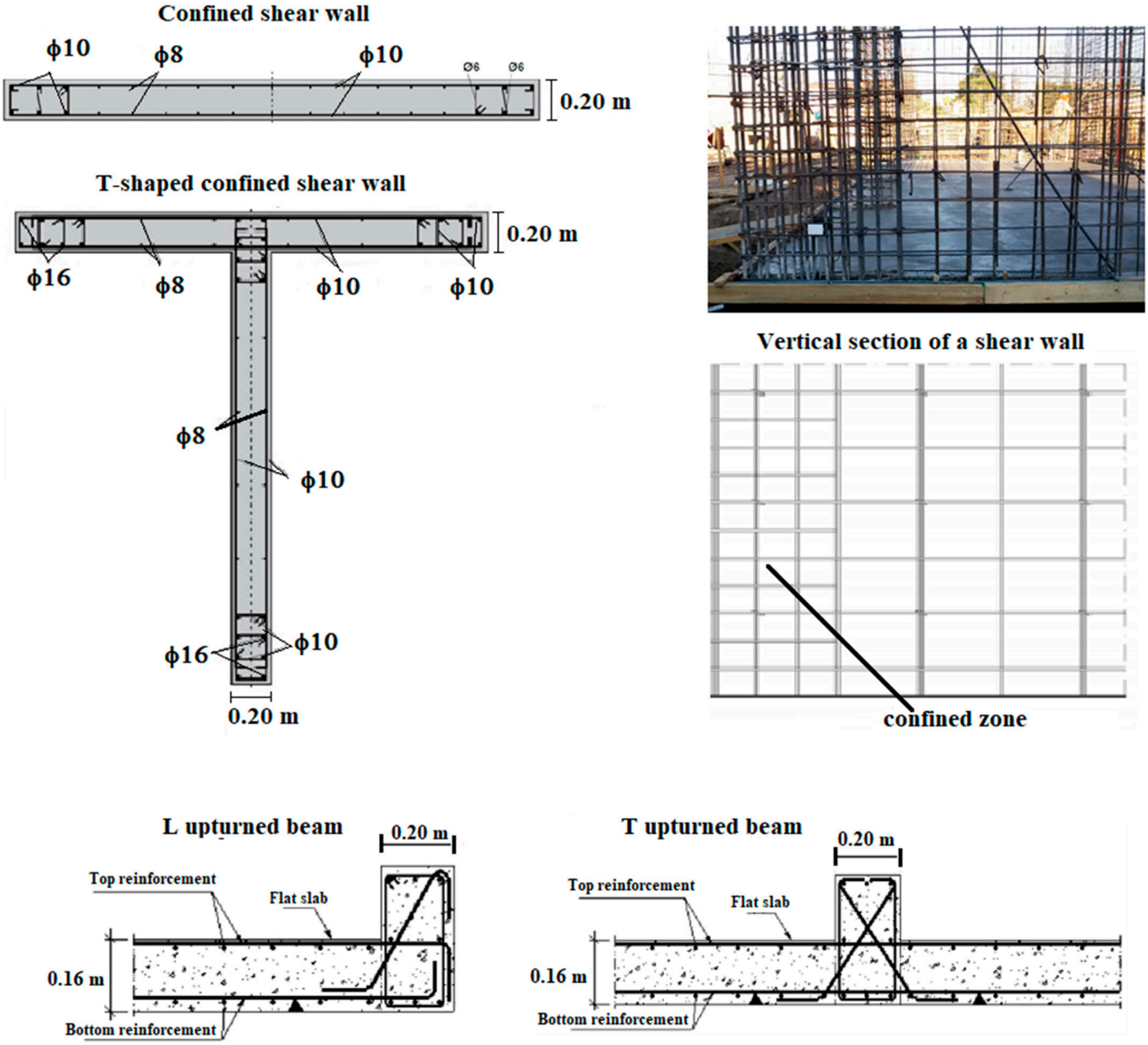

Figure 4. Typical details of the reinforcement of some structural members.

Table 1. Properties of concrete.

Concrete	Structural Part	f_c [MPa]	E [GPa]	ν	γ [kg/m^3]
G20	Foundations and floors Beams and walls from 4° to 6° story	20	23.5	0.2	2500
G25	Beams and walls up to 3° story	25	25.7	0.2	2500

Table 2. Properties of reinforcement steel.

Steel	f_u [MPa]	f_y [MPa]	E [GPa]	ν	γ [kg/m^3]
A630-420H	630	420	200	0.3	7850

Numerical Model

To perform the seismic analyses, the building was modelled by means of the SeismoStruct software [24]. Both walls and beams were modelled with the inelastic force-based

plastic-hinge frame element type infrmFBPH, which features a distributed inelasticity displacement and force-based formulation, concentrating inelasticity within a fixed length of the element [25]. In the element zone where the plastic hinge is assumed to be developed, a fiber distributed plasticity is considered. In other words, in this case the two strategies of concentrated and distributed plasticity are combined leading to a final plastic-hinge-based model. Other approaches use a fiber distributed plasticity involving all the elements (see e.g., [26–28]) or a concentrated plasticity model which do not involve fiber discretization of the elements [13]. Figure 5 provides some instances of fiber discretization of shear walls and upturned beams completed by SeismoStruct. The ASCE/SEI 7–16 [5] recommendations which suggest eliminating any record which does not lead to convergence were also followed. The constitutive models of Mander et al. [29] and of Menegotto and Pinto [30] were adopted for concrete and reinforcing steel, respectively. In Figure 6 are provided the constitutive curves for the reinforcement steel and for the two concrete classes (G20 and G25). The transversal confinement of the concrete core as well as the longitudinal steel bars in walls and beams have been considered in the model by an increase of the concrete strength, according to the Mander model [29].

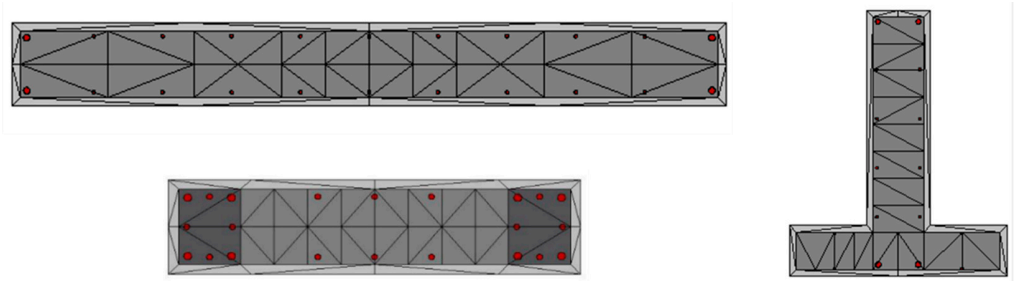

Figure 5. Examples of fiber discretization of shear wall and upturned-beam sections (not to scale, taken from SeismoStruct).

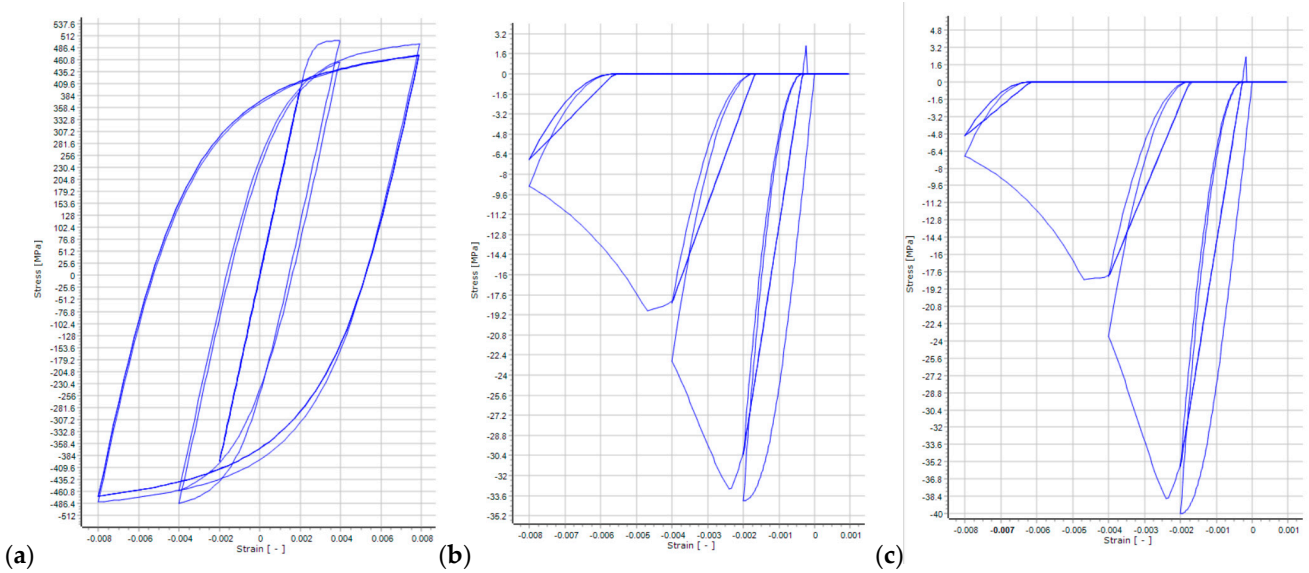

Figure 6. Constitutive curves of (**a**) reinforcement steel, (**b**) G20, and (**c**) G25 concrete as taken from SeismoStruct.

As obtained from a modal analysis of the structure, the first four eigenfrequencies and the related effective masses are given in Table 3, where also the mode types are listed, considering the main effective mass contribution to each mode. The relevant modal shapes are displayed in Figure 7. It is worth noting that the fourth mode is a local mode involving a part of the structure where column-like shear walls are present. This modal shape highlights a structural weakness which may lead to a soft-story collapse mechanism.

Table 3. Eigenfrequencies and effective masses (first four modes).

n.	Mode Type	Freq. [Hz]	Effective Masses [%]					
			Ux	Uy	Uz	Rx	Ry	Rz
1	1st bending y	5.90	1.87	43.23	0.00	25.59	0.62	15.96
2	1st torsional	6.55	4.06	20.07	0.10	12.64	1.01	41.82
3	1st bending x	11.06	56.46	0.00	0.06	0.00	17.24	5.14
4	1st bending z	19.65	0.01	0.33	14.26	4.03	6.62	0.09

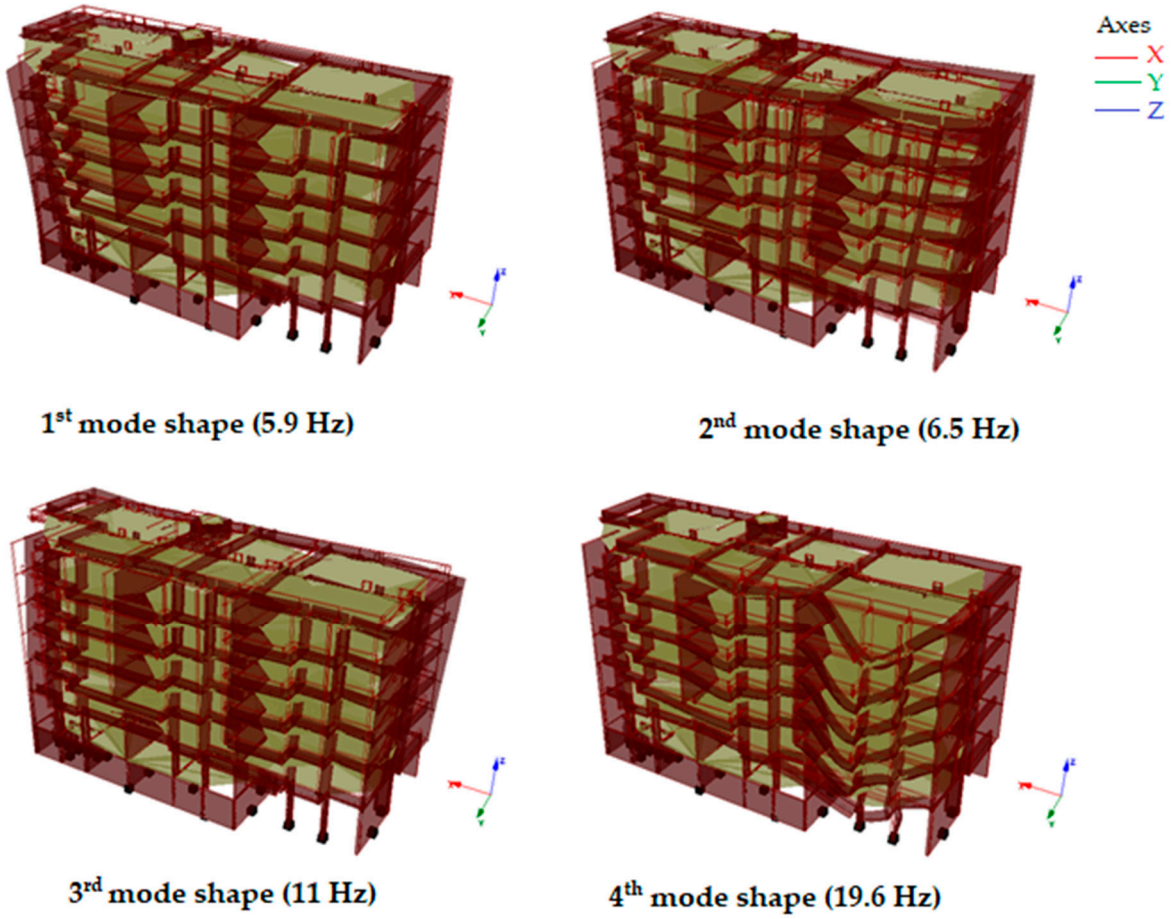

Figure 7. Shapes of the first four modes of the building (a high deformation scale factor is adopted).

3. Design Response Spectra and Spectrum-Consistent Earthquakes

With reference to the Chilean Seismic Code [8], the elastic and reduced design spectra for the X and Y directions are obtained and plotted in Figure 8a,b. The parameters considered for the spectra are listed in the caption of these figures.

According to the Chilean seismic standard, the reduction factors R^*_X and R^*_Y have been calculated through the following equations:

$$R^*_X = 1 + \frac{T_{1X}}{0.10\ T_0 + \frac{T_{1X}}{R_0}}\ ;\ R^*_Y = 1 + \frac{T_{1Y}}{0.10\ T_0 + \frac{T_{1Y}}{R_0}} \quad (1)$$

where T_{1X} and T_{1Y} represent the fundamental periods in the two main directions, T_0 is a characteristic period related to the type of foundation soil, and R_0 is a parameter depending on both the structural typology and the material (for the case-study building $R_0 = 11$). It can be noted that, in contrast to the design spectra obtained through some other national codes like for instance EC8 [4], the elastic and the inelastic spectra derived according to the

Chilean code have different values at zero period. In other words, the reduction factors also affect the part of the spectrum relevant to very stiff oscillators.

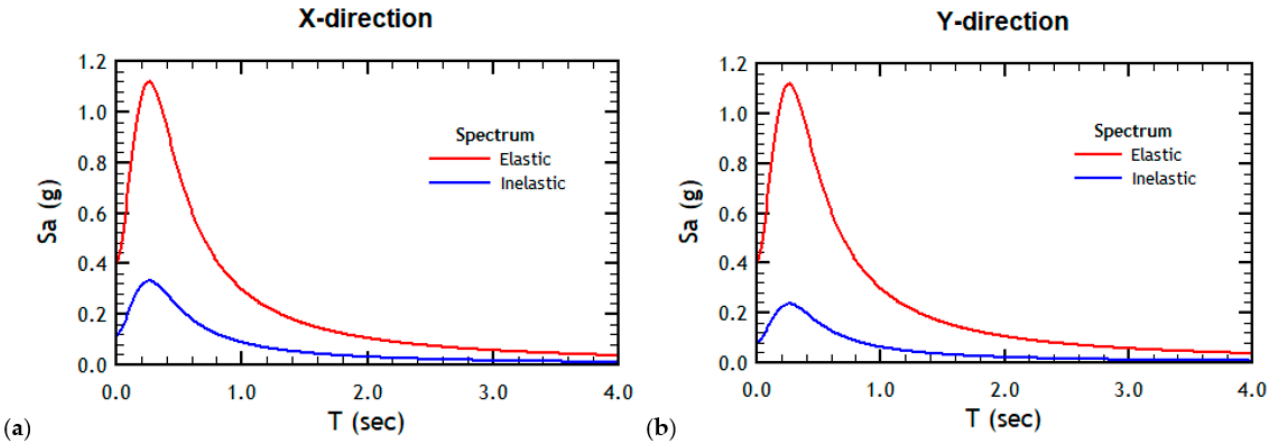

Figure 8. Chilean-code-based elastic (red) and reduced (blue) spectra relevant to Quillota (LAT −32.881 LON −71.244) for the (**a**) X and (**b**) Y components. Parameters used: soil factor S = 1.0; building category I = 1.0; peak ground acceleration a_0 = 3.924 m/s^2; damping ratio ξ = 5%; fundamental periods T_{1x} = 0.0904 s and T_{1y} = 0.1694 s; reductions factors R^*_X = 3.36 and R^*_Y = 4.73.

It is worth noting that the reduced spectra (blue curves) were adopted to perform the MRSA while the LTHA and NLTHA were carried out under a suite of earthquakes consistent with the elastic spectra (red curves).

The spectrum-consistent earthquakes were obtained through the software SeismoMatch [31] by exploiting the CESMD database. According to ACHISINA (Chilean Society for Seismology and Earthquake Engineering) recommendations [32], reference was made to the design elastic spectra in terms of displacements, increased by 17% (see Figure 9). To obtain consistent records, SeismoMatch scales the records, when needed, and/or adds further frequency contents according to the wavelet theory. The length of accelerograms was also cut through the SeismoSignal software [33] by considering a range between 5% and 90% of the Arias Intensity [34]. It is of note that records in both main directions are considered for the matching process, with reference to the elastic design response spectra in the X and Y directions, as usually done [35,36]. In the present case, reference to the displacement elastic spectra is made, the two of them coinciding for the Chilean code, and in fact only one design spectrum appears in Figure 9.

The main characteristics of the ten accelerograms considered in the present investigation are listed in Table 4. In the last column of the table identification codes (Id.) are added to simplify the reference to the earthquakes in the figures.

Table 4. Suite of 10 ground motions consistent with the Chilean response spectra in Figure 8.

Earthquake	Mw	Epicenter Coord.	Station	Id.
Valparaíso 1985	8.0 (CSN) 7.4 (USGS)	33.207° S 71.663° W	Melipilla San Isdro	EQ1 EQ2
Bío-Bío 2010	8.8 (CSN) 8.8 (USGS)	36.122° S 72.898° W	Angol Concepción San Pedro Constitucion Llolleo	EQ3 EQ4 EQ5 EQ6

Table 4. *Cont.*

Earthquake	Mw	Epicenter Coord.	Station	Id.
Coquimbo 2015	8.4 (CSN) 8.3 (USGS)	31.573° S 71.674° W	El Pedregal Tololo San Esteban	EQ7 EQ8 EQ9
Valparaíso 2017	6.9 (CSN) 6.9 (USGS	33.073° S 72.051° W	Torpederas	EQ10

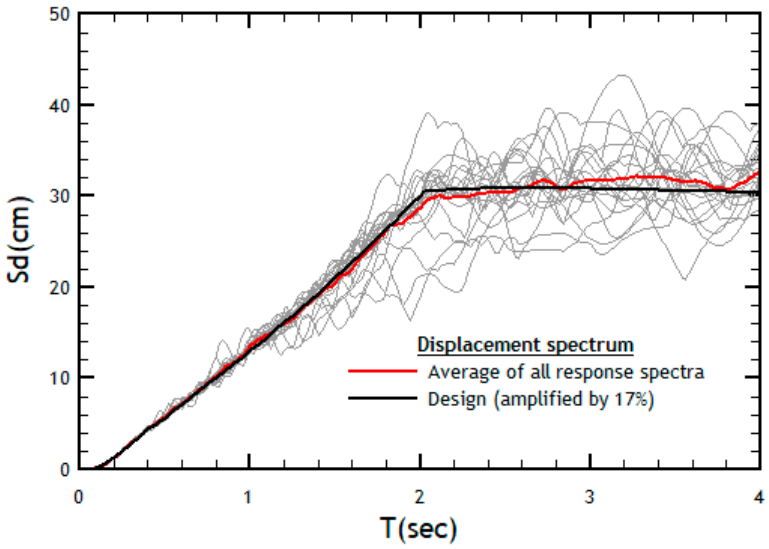

Figure 9. Response spectra of the two components of all the considered records matched with the displacement design spectrum (the same in the two directions) amplified by 17%.

4. Dynamic Linear Analyses

Two kinds of dynamic linear analyses were carried out to assess the peak displacements and the interstory drift demand for the case-study building.

4.1. Modal Response Spectrum Analysis (MRSA)

An MRSA was firstly performed, by referring to the reduced design spectra displayed in Figure 8 (red curves). According to the instructions given by the Chilean code, the contribution of as many modes as needed to reach at least an effective mass of about 90% of the total mass was considered. The maximum displacements along the building height, obtained from the MRSA with reference to the reduced design spectra, are plotted in Figure 10a,b (black dashed lines), respectively relevant to the X and Y directions.

The elastic displacements obtained from the reduced design spectra, say d_{ER_i} (subscript i standing for X and Y, respectively), are expected to be lower than the actual elastic-plastic displacements, say d_{EP_i}, that the structure would experience under earthquakes consistent with the elastic design spectra (blue curves in Figure 7). This is due to two main reasons: (a) displacements d_{ER_i} are obtained with reference to reduced design spectra and (b) displacements d_{ER_i} are obtained through a linear analysis which is not able to directly estimate the inelastic displacement demand when systems with a comparatively short fundamental period (like the case-study building) are concerned.

Therefore, to estimate the actual seismic displacement demand, say d_{EP_i}, the displacements d_{ER_i} should be multiplied by an amplification factor f_i able to fix the above-mentioned (a) and (b) reasons of discrepancy, that is:

$$d_{EP\_i} = f_i \, d_{ER\_i} \; (i = X, Y) \tag{2}$$

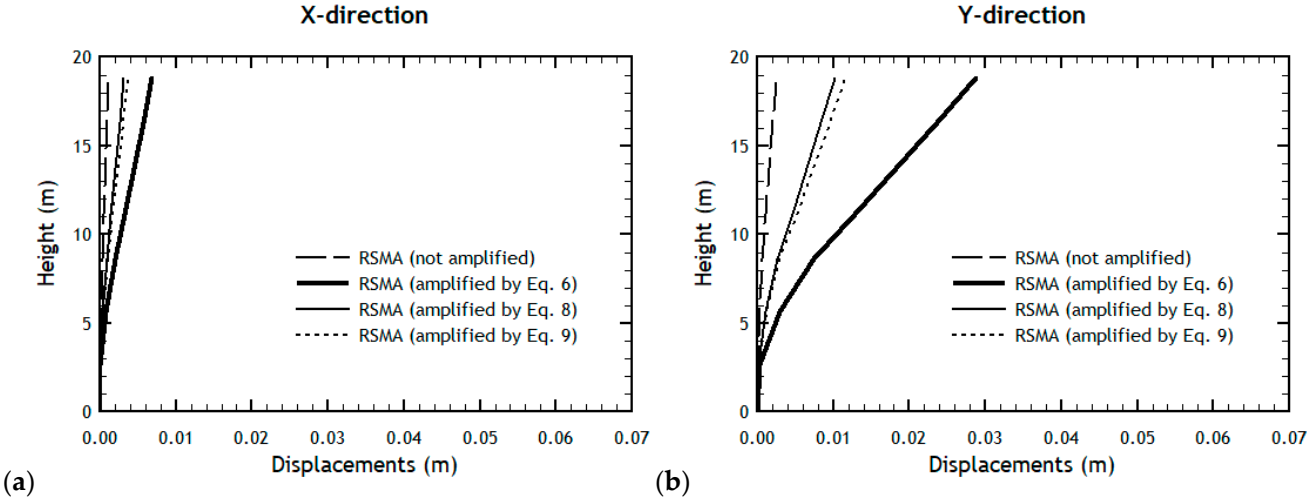

Figure 10. Maximum displacements obtained from the MRSA, with and without amplification factors in the X (**a**) and Y (**b**) directions.

To find a suitable value for f_i, the ED and EE rules [20] could be exploited. According to them, the following empirical formulae apply:

$$\mu_d = r \text{ (flexible oscillators)} \tag{3}$$

$$\mu_d = \frac{r^2 + 1}{2} \text{ (stiffer oscillators)} \tag{4}$$

Equations (3) and (4) relate the global (or displacement) ductility demand $\mu_d = d_{EP}/d_y$ to the reduction factor $r = d_{EL}/d_y$. Here d_y and d_{EP} denote the yield displacement and the maximum displacement of an elastic-plastic oscillator under a given earthquake, while d_{EL} is the maximum displacement of the corresponding elastic oscillator (same natural period in the elastic range) under the given earthquake [37]. Equation (3) applies to sufficiently flexible oscillators (ED rule) while Equation (4) refers to stiffer oscillators (EE rule).

Should d_{yi} and r_i indicate the yield limit and the reduction factor in the i direction, we can reasonably assume that $d_{yi} \equiv d_{ER\_i}$ and $r_i \equiv R_i$, where R_i stands for the reduction factors R_X and R_Y, respectively. In the present study $R_X = 3.36$ and $R_Y = 4.73$ (see Figure 7).

Under the above assumptions, from Equations (3) and (4) it can be finally obtained:

$$f_i = R_i \text{ (flexible oscillators)} \tag{5}$$

$$f_i = \frac{{R_i}^2 + 1}{2} \text{ (stiffer oscillators)} \tag{6}$$

Usually, seismic regulations refer to the amplification factor given by Equation (5) for flexible oscillators, while providing a different value than that given by Equation (6) for stiffer systems. The amplification factors provided by EC8 are for instance:

$$f_i = R_i \; if \; T_{1i} \geq T_C \tag{7}$$

$$f_i = 1 + (R_i - 1)T_C/T_{1i} \; if \; T_{1i} < T_C \tag{8}$$

Here T_{1i} is the fundamental period of the system in the i direction ($i = X$, $i = Y$) while T_C is a characteristic period which delimits the horizontal branch of the EC8 design spectrum. It can be noted that Equations (5) and (7) assign the same value to f_i when flexible enough oscillators are concerned. On the contrary, Equations (6) and (8) lead to rather different values of the amplification factor f_i when stiffer systems are concerned. It is

worth noting that, being $T_C/T_{1i} < 1$, the amplification factor given by EC8 in Equation (8) is lower than that derived from the EE rule and provided by Equation (6).

The SW building considered in the present investigation is a rather stiff system, thus in the present case either Equation (6) or Equation (8) should be applied. Since the shape of the Chilean design spectrum is rather different from that assumed by EC8, the value of the characteristic period T_C to be used in Equation (8) is not a Chilean code design parameter. It can be assumed, however, $T_C = 0.4$ s, this being a reasonable value to distinguish between flexible and stiffer oscillators. The values provided in Table 4 were finally found by applying Equations (6) and (8) in the X and Y directions. It can be noted that the amplification factors obtained by applying Equation (6) are more than double with respect to those given by Equation (8).

For its part, the American code ASCE SEI 7-16 [5] provides the following amplification factor to estimate the inelastic displacements of any system (regardless of whether it is flexible or stiffer) through Equation (2):

$$f_i = \frac{C_{di}}{I_e} \tag{9}$$

In this equation C_d and I_e are respectively the deflection amplification factor and the factor of importance. According to ASCE SEI 7-16, $C_{di} = R_i$ for reinforced concrete shear wall structures while $I_e = 1.2$ for residential buildings. Thus, should reference to ASCE SEI 7-16 be made, the values listed in the last row of Table 5 would apply in the present case.

Table 5. Amplification factors f_X and f_Y obtained from Equations (6) and (8).

Rule	T_{1_X} [s]	T_{1_Y} [s]	R_X	R_Y	f_X	f_Y
EE—Equation (5)	0.17	0.09	3.36	4.73	6.1	11.7
EC8—Equation (7)	0.17	0.09	3.36	4.73	2.79	4.16
ASCE—Equation (8)	0.17	0.09	3.36	4.73	2.8	3.94

Figure 10 plots the results obtained from the MRSA. The dashed-line curves give the displacement demand estimated through the MRSA, without applying any amplification factor. The thinner and the thicker curves are obtained by adopting the amplification factors given by Equations (6) and (8), while the dotted curves refer to Equation (9). It should be noted that the estimates obtained from EC8 and ASCE SEI 7-16 are almost the same. It is worth noting, moreover, that since Chilean regulations [8] do not provide any amplification factor to estimate the inelastic displacements from the elastic values, the dashed-line curve can also be considered as the displacement demand estimated through the Chilean code.

4.2. Linear Time-History Analysis (LTHA)

With reference to a linear model of the building and to the earthquakes referred to in Table 4, a group of ten time-history analyses were performed. The maximum displacements along the building height obtained under the ten earthquakes are displayed in Figure 11a,b, relevant to the X and Y directions. Figure 12a,b provides the interstory drift along the building height. The limit values given by ASCE-SEI 41-17 [38] (red-dashed lines) for the immediate Occupancy (IO), Life Protection (LP), and Collapse Prevention (CP) are also plotted in Figure 11 together with the limit values provided by ACHISINA [32] (purple dotted-dashed lines) relevant to fragile and ductile partitions. It can be noted that the code-based limits are not overcome, either on average or under any of the considered earthquakes.

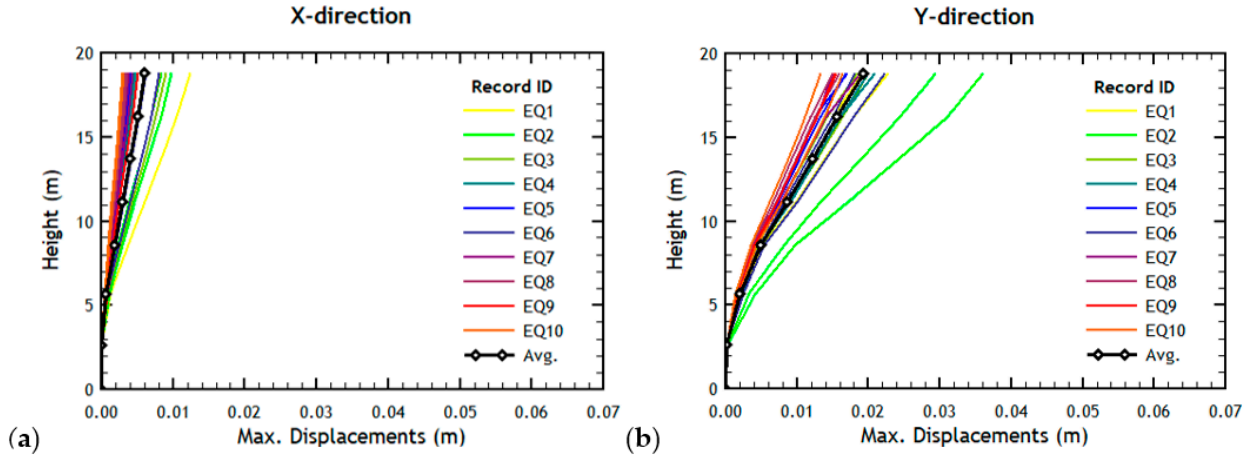

Figure 11. Maximum displacements in (**a**) X-direction and (**b**) Y-direction, as obtained from THLA for the records of Table 3.

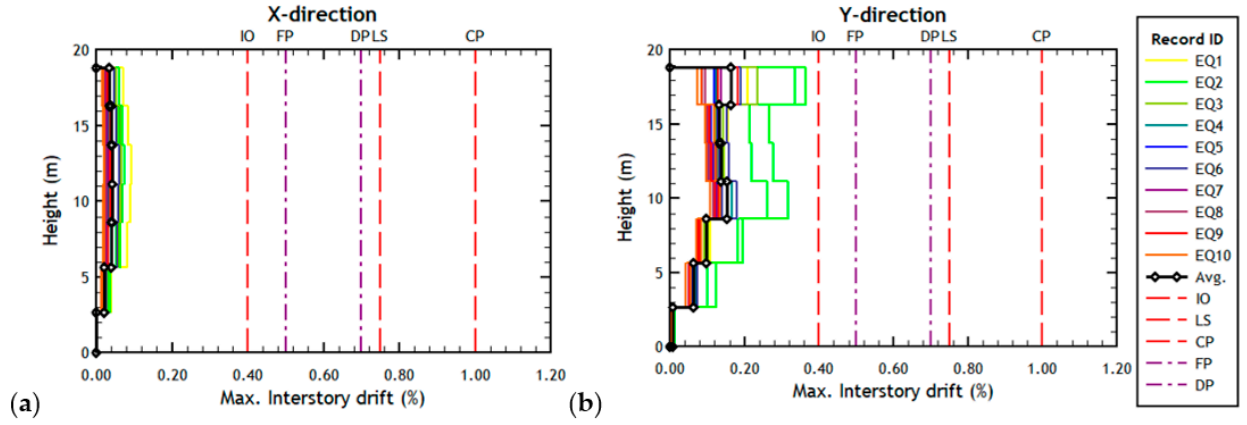

Figure 12. Interstory drift in (**a**) X-direction and (**b**) Y-direction, as obtained from THLA for the earthquakes in Table 3. The ASCE-SEI 41-17 (red dashed vertical lines) and ACHISINA limits (purple dash-dot vertical lines) are plotted in the figure for IO (immediate occupancy), LS (Life Safety), CP (Collapse Prevention), FP (Fragile partitions), and DP (Ductile Partitions).

5. Results of the Non-Linear Time-History Analysis (NLTHA)

An NLTHA was performed under each of the ten earthquakes listed in Table 4. The results in terms of maximum displacements and interstory drift in the two main directions are provided in Figures 13 and 14. The curves obtained averaging the results are also plotted in the diagrams (black lines with circles). The limit values for the interstory drift given by ASCE-SEI 41-17 [38] (red-dashed lines) and by ACHISINA [32] (purple dotted-dashed lines) are plotted in the diagrams of Figure 13.

The results of the NLTHA show again that the building is much stiffer in the X direction than in the Y direction. The interstory drifts in the *X* direction are considerably lower than the thresholds set by both the ASCE SEI 41-17 and the ACHISINA Manual. On the contrary, the IO limit set by ASCE SEI 41-17 was overcome under some of the earthquakes in the *Y* direction. In the same direction the limit given by ACHISINA for buildings with fragile partitions is reached under the strongest earthquake of the set. Since, however, both ASCE SEI 41-17 and ACHISINA Manual allow considering the values of displacements and drifts averaged over the ten earthquakes of the set, it is of note that the code limits are safely respected in the two directions when the averaged results are considered. This highlights an overall good performance of the structure.

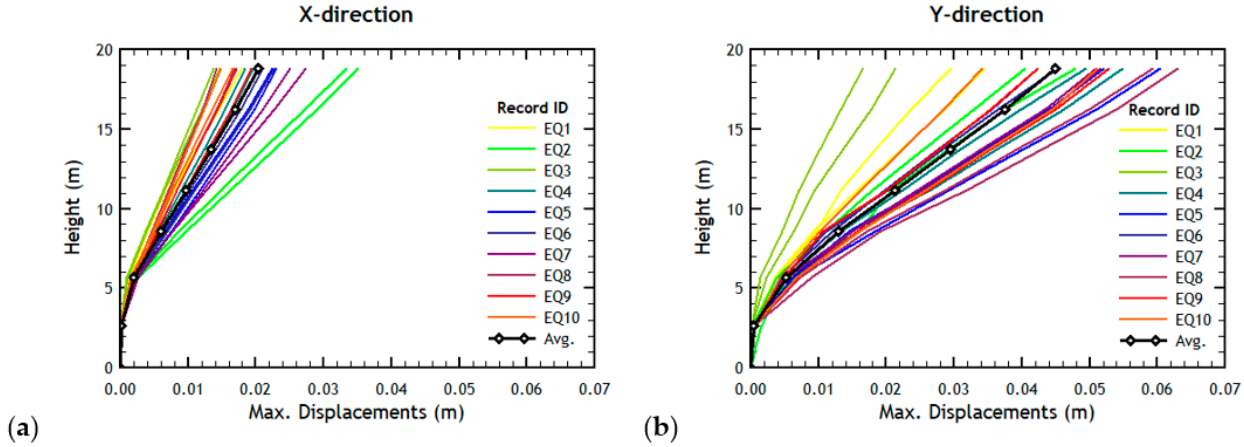

Figure 13. Maximum displacements in (**a**) X-direction and (**b**) Y-direction, as obtained from NLTHA for the records of Table 3.

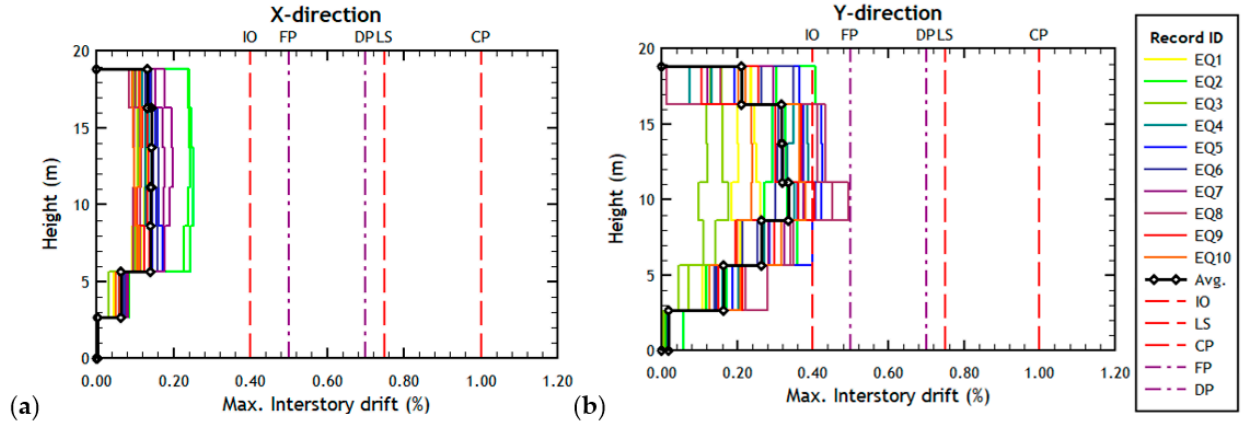

Figure 14. Interstory drift in (**a**) X-direction and (**b**) Y-direction, as obtained from NLTHA for the earthquakes in Table 3. The ASCE-SEI 41-17 (red dashed vertical lines) and ACHISINA limits (purple dash-dot vertical lines) are also plotted in the figure. IO (immediate occupancy), LS (Life Safety), CP (Collapse Prevention), FP (Fragile Partitions), and DP (Ductile Partitions).

6. Comparing the Results from Linear and Non-Linear Analyses

Table 6 presents a comparison between the peak displacements (taken at the top of the building) and the maximum interstory drift values obtained through the linear and non-linear analyses. The first four rows provide the results taken from the MRSA: not amplified, amplified by Equation (6), by Equation (8), and by Equation (9). The values averaged over the ten earthquakes for linear and non-linear time-history analyses are provided in the last two rows of the same table. It can be noted that the values obtained from the linear analyses (MRSA and LTHA) are always lower than the actual values obtained through the NLTHA, even when amplified according with conventional or code factors.

The NLTHA is here assumed to give the more realistic values, this kind of analysis being the most complete one, based as it is on the integration of the elastic-plastic differential equations of motion under the given earthquakes. Under this assumption, the results obtained from the NLTHA, averaged over the ten earthquakes, are taken as the reference (actual) values. The comparison presented in Table 6 shows that, when not amplified, the displacements predicted through the MRSA may be almost twenty times lower than the actual ones (NLTHA average). When amplified by the factor given by Equation (6), they are from 1.5 to 3 times lower than the actual ones; when amplified by Equation (8) according to EC8, or by Equation (9) according to ASCE SEI 41-17, they are from 4 to more than 6 times lower than the actual ones.

Table 6. Maximum displacement and interstory drift from the analyses in the two directions.

Analysis	Peak Top Displacement (m)		Interstory Drift (%)	
	X dir.	Y dir.	X dir.	Y dir.
MRSA (not amplified)	0.0011	0.0025	0.0083	0.0184
MRSA amplified by Equation (6)	0.0068	0.0287	0.0505	0.2152
MRSA amplified by Equation (8)	0.0031	0.0102	0.0231	0.0765
MRSA amplified by Equation (9)	0.0038	0.0116	0.0278	0.0869
LTHA (average)	0.0066	0.0193	0.0597	0.1352
NLTHA (average)	0.0204	0.0450	0.1422	0.3240

In Table 7 the discrepancy δ between the linear and non-linear displacement demand prediction is also provided, calculated by means of the following ratio:

$$\delta = \frac{D_L - D_{NL}}{D_{NL}} \times 100 \tag{10}$$

here D_L and D_{NL} denote respectively the values obtained from the linear and the non-linear analyses. An error ranging from about 33% to about 95% was found (the minus sign meaning that the linear analysis underestimates the actual displacement demand with respect to the non-linear one).

Table 7. Discrepancy δ calculated by means of Equation (10).

Analysis	δ for Peak Top Displacement (%)		δ for Interstory Drift (%)	
	X dir.	Y dir.	X dir.	Y dir.
MRSA (not amplified)	−94.6	−94.4	−94.2	−94.3
MRSA amplified by Equation (6)	−66.7	−36.2	−64.5	−33.6
MRSA amplified by Equation (8)	−84.8	−77.3	−83.8	−76.4
MRSA amplified by Equation (9)	−81.4	−74.2	−80.5	−73.2
LTHA (average)	−67.6	−57.1	−58.0	−58.3

A comparison of the results is also presented in Figures 15–18, showing in a clearer way that the linear analyses are always in defect compared to the non-linear analyses. Even when amplified according to the EE rule or to the EC8 or ASCE SEI 41-17 provisions, the results of the MRSA strongly underestimate the actual displacement demand. The LTHA was shown to also be unable to predict the actual displacement demand, underestimating it even by more than 50–60%.

As an instance, a comparison of the top displacement time-histories obtained from the linear and non-linear analysis under one of the most violent earthquakes of the set is shown in Figure 19. The diagrams show a higher displacement demand in the weaker Y direction, the actual inelastic demand (detected by the non-linear analysis) being in fact much higher than that found through the linear analysis.

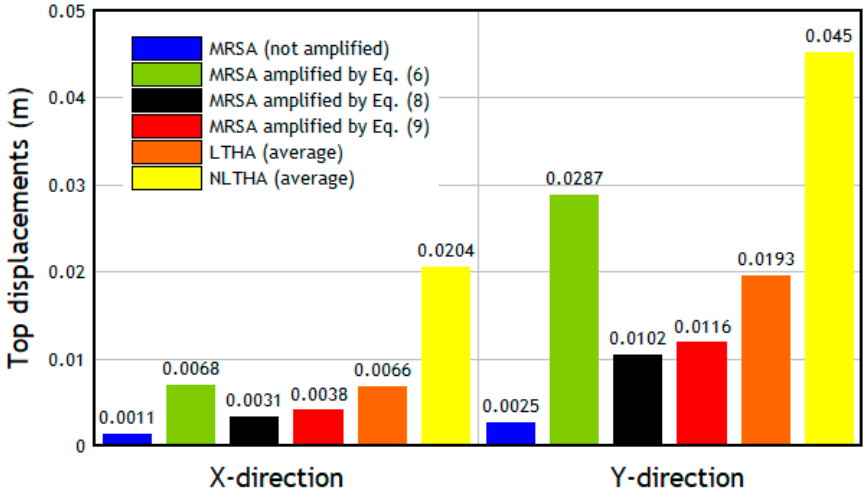

Figure 15. Histogram with the maximum displacements predicted by the different analyses.

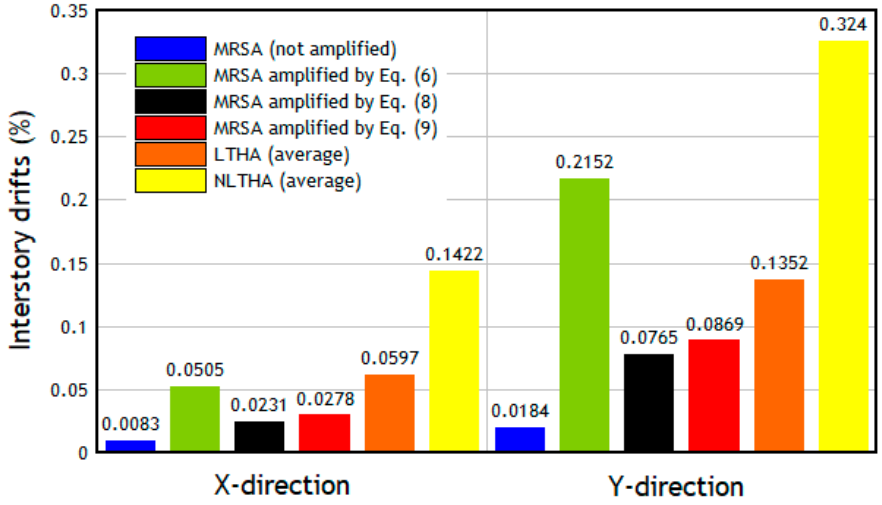

Figure 16. Histogram with the interstory drifts predicted by the different analyses.

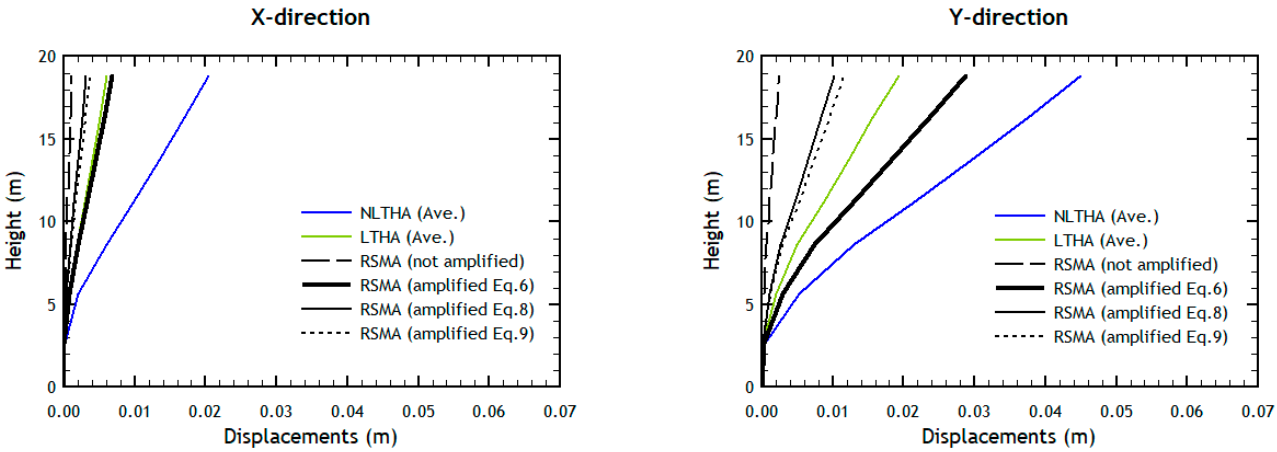

Figure 17. Maximum displacements as predicted by the different analyses.

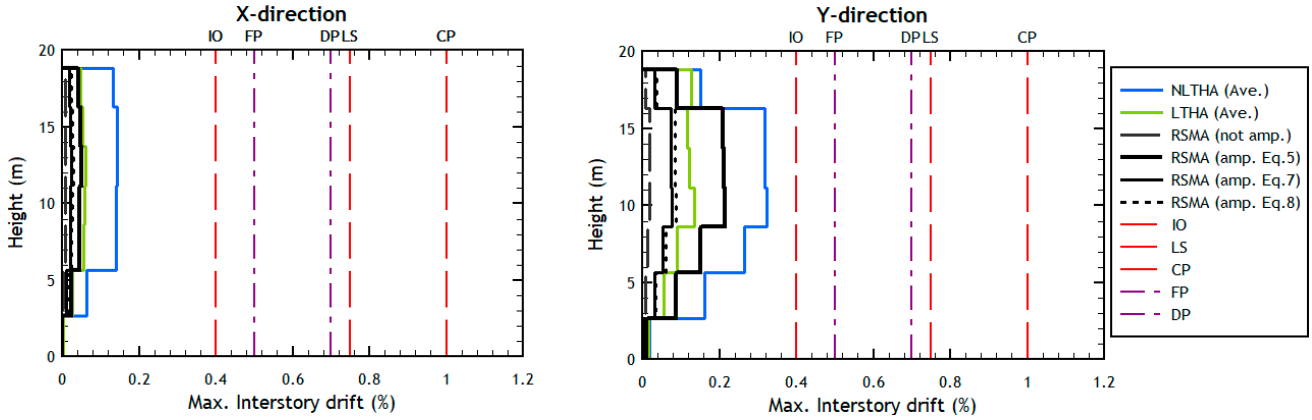

Figure 18. Interstory drifts obtained from the different types of analyses. ASCE-SEI 41-17 (red dashed vertical lines) and ACHISINA limits (purple dash-dot vertical lines) are also plotted.

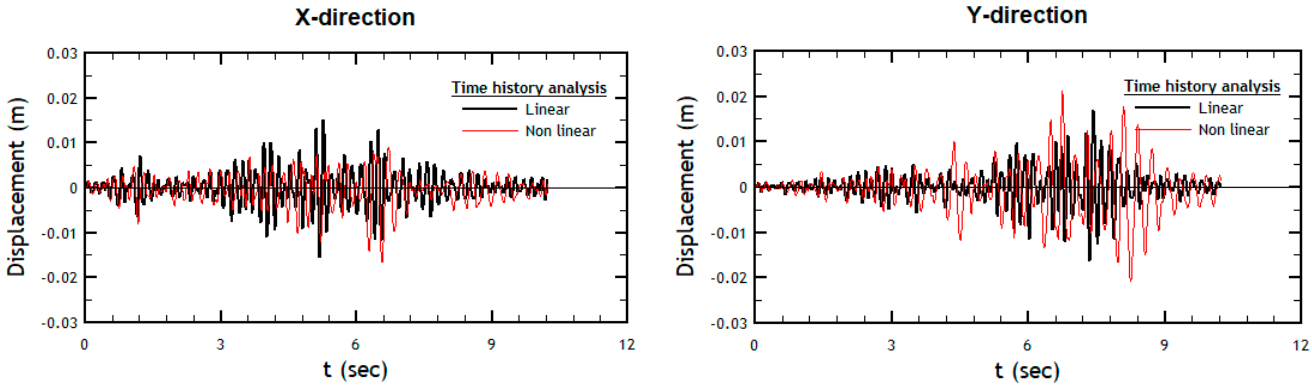

Figure 19. Comparison of top displacements achieved under the Valparaiso earthquake (24 April 2017, registered in Torpederas Station).

7. Post-Elastic Behavior

The non-linear analysis is very useful to assess the most demanded zones of the structure. This knowledge is of paramount importance because it leads to an understanding of the collapse mechanisms of the building and the global and local ductility demand. Figure 20 shows where the plastic hinges developed in the case-study building under the strongest ground motion of the set. The plastic hinges were located almost all in the beams, which is in fact a good structural behavior, according to the strength hierarchy philosophy. However, it can be noted that a plastic hinge formed also at the base of one of the weaker walls on the right side of the building. This may be rather dangerous since a local soft-story mechanism can be triggered, although the rest of the structure is not involved due to the redundant design of all the other walls.

The risk of a soft-story mechanism was also predicted by the modal analysis of the structure, where the fourth mode highlighted the local weakness due to the presence of column-like shear walls at the base of the right part of the structure (see Figure 7). It was found that, even though the global ductility demand is similar for weaker and stronger walls, the local ductility demand (curvature ductility) is higher for the weaker walls [21]. An increase of the local ductility demand in such structural elements means more demanding design and detailing requirements to ensure a sufficient local ductility capacity.

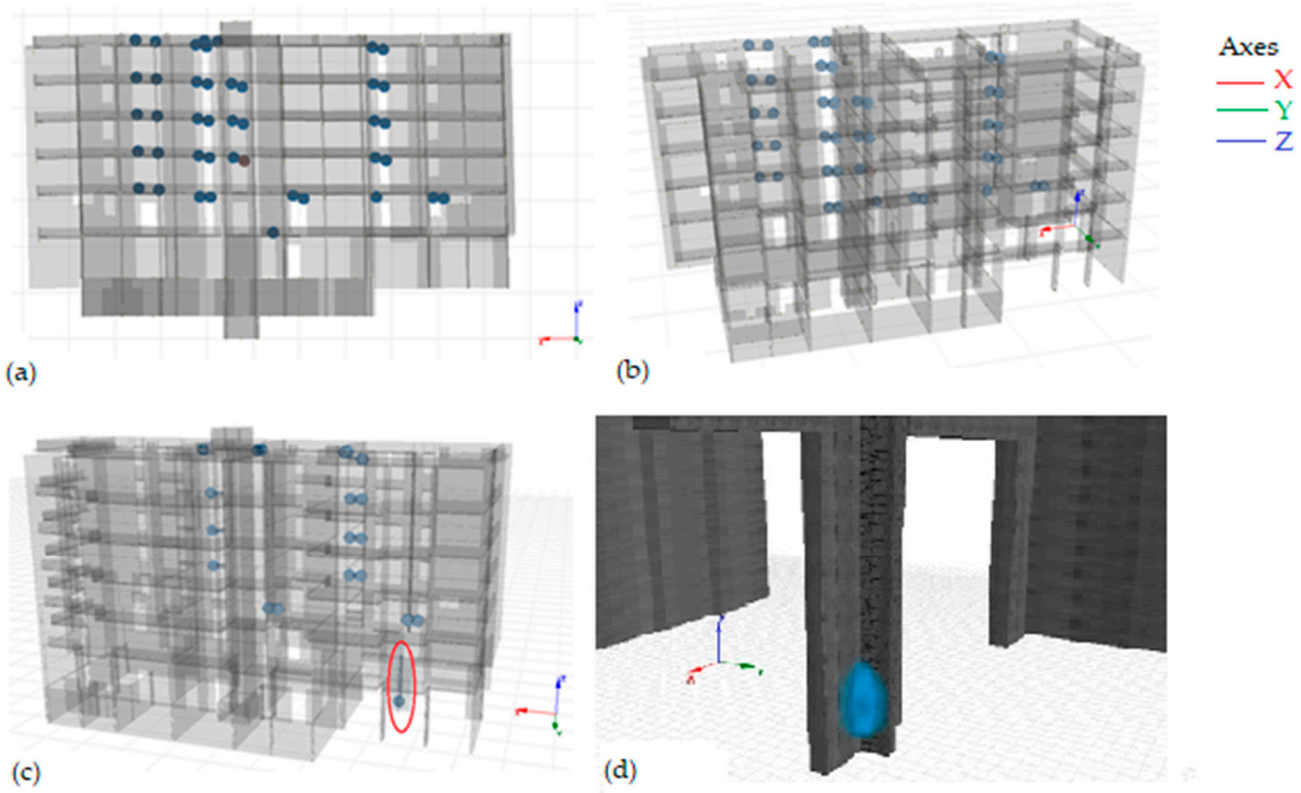

Figure 20. (**a**,**b**) Plastic hinges detected in the model during the non-linear dynamic analysis; (**c**,**d**) plastic hinge at the base of a weaker column on the right side of the building.

8. Concluding Remarks

The paper presented a numerical study aimed at investigating the reliability of code-compliant linear and non-linear dynamic analyses to assess the seismic performance of reinforced-concrete shear-wall (RC-SW) buildings. The interest of the study relies on the fact that RC-SW buildings are widely used in earthquake-prone countries like Chile, where seismic rules only refer to linear methods of analysis, without providing suitable corrective factors to estimate the actual inelastic displacement demand. It should be considered, on the other hand, that linear analyses are generally unable to give a suitable assessment of the displacement demand of comparatively stiff structures like RC-SW buildings under strong earthquakes.

With reference to a case-study mid-rise building recently built in Chile and designed according to the current Chilean regulations, the study showed that the code-compliant linear analyses (MRSA and LTHA) can lead to underestimating the actual displacement demand in RC-SW buildings. The discrepancy between the maximum displacements and the interstory drifts predicted by the MRSA (the only kind of analysis to which the current Chilean code refers) may be very high indeed. The errors may range from 33% when amplification factors based on the well-known equal-energy rule are applied to more than 90% when no amplification factors are adopted at all (according to the present Chilean code provisions). Even when the corrective formulas proposed by the European Codes or by the ASCE SEI 7-12 are applied, the MRSA was found to underestimate the actual values from 4 to 6 times. This also confirms the very conventional nature of the behavior (reduction) factor for these kinds of structures.

The present study also warns against the danger of local soft-story mechanisms that may affect shear-wall buildings when lower-stiffness walls are present among the much stiffer ones. It must be stressed, however, that only one of the walls of the considered building was found to be affected by damage under severe ground motions, while the

redundancy of the other shear walls was able to prevent bad global collapse mechanisms involving plastic hinges in the vertical structural elements. Moreover, it is worth noting that the case-study building showed an overall good seismic performance, as well-designed RC-SW structures are in fact expected to have. The peak displacements and interstory drifts in the two main directions were found to be lower, on average, than the limits imposed by ASCE SEI 7-12 and ACHISINA.

Although the results presented in the paper are relevant to a specific RC-SW building, it should be noted that it represents the typical mid-rise residential Chilean building, which leads to a likely generalization of the findings discussed in the paper. Further parametric studies on different RC-SW buildings are however needed to propose suitable strategies to enhance the code provisions. The aim of the present investigation was to give preliminary insights on some critical issues which may lead to unsafe design of RC-SW buildings when referring to current code rules. The results presented can contribute to the improvement of the seismic design and assessment of RC-SW buildings which are in general excellent earthquake-resistant structures.

Author Contributions: Conceptualization, methodology, writing—review, and supervision, M.C.P. and J.C.V.P.; software, G.P., D.O.B. and J.C.V.P.; validation, G.P., J.C.V.P. and M.C.P.; investigation, M.C.P., J.C.V.Q. and G.P. All authors have read and agreed to the published version of the manuscript.

Funding: This research was funded by Agencia Nacional de Investigación y Desarrollo (ANID Chile), grant number FOVI 210063.

Data Availability Statement: The data will be made available on request.

Acknowledgments: Second and forth author would like to acknowledge the Pontificia Universidad Católica de Valparaíso for supporting this research. The GLOBUS Program and the Visiting Professor Program of the University of Cagliari (Italy) are also acknowledged by the authors. The paper has been developed in the framework of a bilateral agreement between the University of Valparaiso (Chile) and the University of Cagliari (Italy). The authors acknowledge accessing strong-motion data through the Center for Engineering Strong Motion Data (CESMD), last visited on 23 Jun 2020. The networks or agencies providing the data used in this report are the California Strong Motion Instrumentation Program (CSMIP) and the USGS National Strong Motion Project (NSMP).

Conflicts of Interest: The authors declare no conflict of interest.

References

1. Fintel, M. Performance of buildings with shear walls in earthquakes of the last thirty years. *PCI J.* **1995**, *40*, 62–80. [CrossRef]
2. Ugalde, D.; Lopez-Garcia, D. Behavior of reinforced concrete shear wall buildings subjected to large earthquakes. *Procedia Eng.* **2017**, *199*, 3582–3587. [CrossRef]
3. Ugalde, D.; Lopez-Garcia, D. Analysis of the seismic capacity of Chilean residential RC shear wall buildings. *J. Build. Eng.* **2020**, *31*, 101369. [CrossRef]
4. European Committee for Standardization (CEN). *EN 1998-3: Eurocode 8: Design of Structures for Earthquake Resistance*; CEN: Brussels, Belgium, 2004.
5. *ASCE/SEI 7-16*; Minimum Design Loads and Associated Criteria for Buildings and Other Structures. ASCE (American Society of Civil Engineers): Reston, VA, USA, 2016.
6. *FEMA P-695*; Quantification of Building Seismic Performance Factors. FEMA (Federal Emergency Management Agency): Washington, DC, USA, 2009.
7. *FEMA P-58-2*; Seismic Performance Assessment of Buildings-Implementation Guide. FEMA (Federal Emergency Management Agency): Washington, DC, USA, 2012.
8. *NCh433Of.1996*; Diseño Sísmico de Edificios, Norma Chilena Oficial. Last Version Realeased in 2009; INN (Instituto Nacional de Normalización): Santiago, Chile, 2012. (In Spanish)
9. Porcu, M.C. Ductile behavior of timber structures under strong dynamic loads. In *Wood in Civil Engineering*; InTechOpen: Rijeka, Croatia, 2017; pp. 173–196.
10. Vielma, J.C.; Mulder, M.M. Improved procedure for determining the ductility of buildings under seismic loads. *Rev. Int. Métodos Numéricos Para Cálculo Diseño Ing.* **2018**, *34*, 1–27.
11. Vielma, J.C.; Barbat, A.H.; Oller, S. Seismic safety of low ductility structures used in Spain. *Bull. Earthq. Eng.* **2010**, *8*, 135–155. [CrossRef]

12. Porcu, M.C.; Bosu, C.; Gavrić, I. Non-linear dynamic analysis to assess the seismic performance of cross-laminated timber structures. *J. Build. Eng.* **2018**, *19*, 480–493. [CrossRef]
13. Porcu, M.C.; Vielma, J.C.; Panu, F.; Aguilar, C.; Curreli, G. Seismic Retrofit of Existing Buildings Led by Non-Linear Dynamic Analyses. *Int. J. Saf. Secur. Eng.* **2019**, *9*, 201–212. [CrossRef]
14. Porcu, M.C. Code inadequacies discouraging the earthquake-based seismic analysis of buildings. *Int. J. Saf. Secur. Eng.* **2017**, *7*, 545–556.
15. Vielma, J.C.; Porcu, M.C.; López, N. Intensity Measure Based on a Smooth Inelastic Peak Period for a More Effective Incremental Dynamic Analysis. *Appl. Sci.* **2020**, *10*, 8632. [CrossRef]
16. Vielma, J.C.; Porcu, M.C.; Gomez-Fuentes, M.A. Non-linear analyses to assess the seismic performance of RC buildings retrofitted with FRP. *Rev. Int. Métodos Numéricos Para Cálculo Diseño Ing.* **2020**, *36*. Available online: https://www.scipedia.com/public/Vielma-Perez_et_al_2019a (accessed on 15 December 2021).
17. Kelly, T. Nonlinear analysis of reinforced concrete shear wall structures. *Bull. N. Z. Soc. Earthq. Eng.* **2004**, *37*, 156–180. [CrossRef]
18. Ile, N.; Reynouard, J.M. Nonlinear analysis of reinforced concrete shear wall under earthquake loading. *J. Earthq. Eng.* **2000**, *4*, 183–213. [CrossRef]
19. Hidalgo, P.A.; Jordan, R.M.; Martinez, M.P. An analytical model to predict the inelastic seismic behavior of shear-wall, reinforced concrete structures. *Eng. Struct.* **2002**, *24*, 85–98. [CrossRef]
20. Miranda, E.; Bertero, V. Evaluation of Strength Reduction Factors for Earthquake-Resistant Design. *Earthq. Spectra* **1994**, *10*, 357–379. [CrossRef]
21. Lestuzzi, P.; Badoux, M. An Experimental Confirmation of the Equal Displacement Rule for RC Structural Walls. Available online: http://citeseerx.ist.psu.edu/viewdoc/download?doi=10.1.1.122.7970&rep=rep1&type=pdf (accessed on 15 December 2021).
22. Porcu, M.C.; Montis, E.; Saba, M. Role of model identification and analysis method in the seismic assessment of historical masonry towers. *J. Build. Eng.* **2021**, *43*, 103–114. [CrossRef]
23. Echeverría, M.J.; Jünemann, R. Characterization of fish-bone type RC walls buildings through analytical fragility functions. In Proceedings of the 17th World Conference on Earthquake Engineering, Sendai, Japan, 13–18 September 2020.
24. Seismosoft. SeismoStruct 2018—A Computer Program for Static and Dynamic Nonlinear Analysis of Framed Structures. Available online: http://www.seismosoft.com (accessed on 15 December 2021).
25. Scott, M.H.; Fenves, G.L. Plastic hinge integration methods for force-based beam–column elements. *J. Struct. Eng.* **2006**, *132*, 244–252. [CrossRef]
26. Furinghetti, M.; Pavese, A. Definition of a Simplified Design Procedure of Seismic Isolation Systems for Bridges. *Struct. Eng. Int.* **2020**, *30*, 381–386. [CrossRef]
27. Vielma, J.C.; Barbat, A.H.; Oller, S. Seismic performance of buildings with waffled-slab floors. *ICE Proc. Struct. Build.* **2009**, *162*, 169–182. [CrossRef]
28. Barbat, A.H.; Oller, S.; Mata, P.; Vielma, J.C. Computational simulation of the seismic response of buildings with energy dissipating devices. In *Computational Structural Dynamics and Earthquake Engineering: Structures and Infrastructures Book Series, 2008, 2 (Structures and Infrastructures)*; Taylor & Francis Ltd.: London, UK, 2008; ISBN 978-04-154-5261-8.
29. Mander, J.B.; Priestley, J.N.; Park, R. Theoretical Stress-Strain Model for Confined Concrete. *J. Struct. Eng.* **1988**, *114*, 1804–1826. [CrossRef]
30. Menegotto, M.; Pinto, P.E. Method of Analysis for Cyclically Loaded R.C. Plane Frames including Changes in Geometry and Non-Elastic Behaviour of Elements under Combined Normal Force and Bending. Available online: https://www.e-periodica.ch/cntmng?pid=bse-re-001:1973:13::9 (accessed on 15 December 2021).
31. Seismosoft. SeismoMatch—A Computer Program for Spectrum Matching of Earthquake Records. 2018. Available online: https://www.seismosoft.com (accessed on 1 August 2020).
32. ACHISINA. Alternative Procedure for the Seismic Analysis and Design of Tall Buildings, Santiago (Chile). 2017. Available online: http://www.achisina.cl/images/PBD/ACHISINA (accessed on 1 August 2020).
33. Seismosoft. SeismoSignal-A Computer Program for Signal Processing of Time-Histories. 2018. Available online: https://www.seismosoft.com (accessed on 1 August 2020).
34. Arias, A. A measure of earthquake intensity. In *Seismic Design for Nuclear Power Plants*; Hansen, R.J., Ed.; MIT Press: Cambridge, MA, USA, 1970; pp. 438–483.
35. Furinghetti, M.; Pavese, A. Equivalent Uniaxial Accelerogram for CSS-Based Isolation Systems Assessment under Two-Components Seismic Events. *Mech. Based Des. Struct. Mach.* **2017**, *45*, 282–295. [CrossRef]
36. Vielma, J.C.; Aguiar, R.; Frau, C.; Zambrano, A. Irregularity of the Distribution of Masonry Infill Panels and Its Effect on the Seismic Collapse of Reinforced Concrete Buildings. SI: Seismic Assessment and Design of Structures. *Appl. Sci.* **2021**, *11*, 8691. [CrossRef]
37. Chopra, A.K. Dynamics of structures. In *Theory and Applications to Earthquake Engineering*; Prentice Hall: Hoboken, NJ, USA, 2001.
38. *ASCE/SEI 41-17*; Seismic Evaluation and Retrofit of Existing Buildings. American Society of Civil Engineers: Reston, VA, USA, 2017.